High-Speed and Uninterrupted Communication for High-Speed Trains by Ultrafast WDM Fiber–Wireless Backhaul System

Pham Tien Dat, *Member, IEEE*, Atsushi Kanno, *Member, IEEE*, Keizo Inagaki, François Rottenberg, *Member, IEEE*, Naokatsu Yamamoto, and Tetsuya Kawanishi, *Fellow, IEEE*

(Post-Deadline Paper)

***Abstract*—We developed a high-speed and handover-free communication network for high-speed trains (HSTs) using an ultrafast and switchable wavelength-division multiplexing fiber–wireless backhaul system in the W band. We successfully transmitted approximately 20-Gb/s and 10-Gb/s signals over the switched fiber–wireless links in the downlink and uplink directions, respectively. An ultrafast radio-cell switching of less than 10 μs was experimentally demonstrated in both downlink and uplink directions. Moreover, the possibility of connecting a central station to many remote radio cells was evaluated, confirming that an uninterrupted communication network up to several tens of kilometers can be achieved for HSTs. The proposed system can overcome the current challenges in mobile networks and can provide a potential solution for the provision of advanced services to users on HSTs in future 5G and beyond networks.**

***Index Terms*—Fiber–wireless convergence, high-speed train, mobile backhaul, moving cell, radio-over-fiber.**

I. Introduction

PROVIDING advanced services, such as high-definition televisions, online gaming, interacting with social clouds, or video conferences, to moving users is one of the challenges of mobile networks. Currently, fast-moving users still need to transfer to large radio cells, which considerably reduces the communication throughput [1]. To provide advanced services to fast-moving users, such as passengers on high-speed trains (HSTs), gigabit-level communications and thus new broadband communication systems are required. However, many challenges, such as high penetration loss, fading, and frequent handovers, must be overcome to construct such a high-speed network. HSTs are considered one of the verticals in 5G and beyond networks and have been discussed in the Third Generation Partnership Project (3GPP) 5G New Radio [2], [3] and ITU-R [4]. Among the solutions proposed by 3GPP [5], a dedicated moving relay node is considered cost effective to serve data-intensive users on HSTs [6]. In this approach, separated backhaul systems and access networks are considered. Using this method, the penetration loss and the shadowing effects can be avoided and the number of handovers can be reduced. However, it is difficult to increase the transmission capacity to end users because of the bottlenecks in the backhaul systems. The relay network also requires mobility management between remote units, which significantly increases the system complexity and management. Moreover, in these networks, all remote units are required to be activated at the same time, which considerably increases the power consumption and interference between radio cells. The backhaul systems should operate in high-frequency bands for increasing the transmission capacity and avoiding the interference with other mobile networks, which are likely to be deployed in the millimeter-wave (mmWave) bands in 5G and beyond networks [7], [8].

A cell-less and user-centric network has been recently proposed to solve handover problems and improve the resource allocation and management in 5G networks, especially for fast-moving users [9]. Nevertheless, many challenges, including the complexity of the network control and the transmission of control signals over the backhaul networks, remain to be overcome to obtain such a network. For cellular networks for HSTs, however, such a network can be realized easily using a linear-cell network configuration [10]. Advanced photonic technologies, such as fast wavelength switching and convergence of fiber-optic and wireless systems in high-frequency bands, can also be utilized. Radio-over-fiber (RoF) and distributed antenna systems have been proposed for HST communications [11]–[14]. However, the use of wireless backhauls in the microwave band limits the transmission capacity. The inclusion of media converters at the interface of fiber and wireless systems also significantly increases the transmission latency and power consumption. Recently, we proposed a high-speed backhaul network for HSTs using a seamless wavelength-division multiplexing

Manuscript received July 14, 2018; revised October 25, 2018 and December 2, 2018; accepted December 3, 2018. Date of publication December 7, 2018; date of current version February 1, 2019. This work was supported in part by the "Research and development for expansion of radio wave resources," by the Ministry of Internal Affairs and Communications, Japan, and in part by JSPS KAKENHI under Grant 18K04156. *(Corresponding author: Pham Tien Dat.)*

P. T. Dat, A. Kanno, K. Inagaki, and N. Yamamoto are with the Network System Research Institute, National Institute of Information and Communication Technology, Tokyo 184-0015, Japan (e-mail: ptdat@nict.go.jp; kanno@nict.go.jp; k-inagaki@nict.go.jp; naokatsu@nict.go.jp).

F. Rottenberg is with the ICTEAM Institute, Universite Catholique de Louvain, Louvain-la-Neuve 1348, Belgium (e-mail: francois.rottenberg@uclouvain.be).

T. Kawanishi is with the School of Fundamental Science and Engineering, Waseda University, Tokyo 169-8050, Japan (e-mail: kawanishi@waseda.jp).

Color versions of one or more of the figures in this paper are available online at http://ieeexplore.ieee.org.

Digital Object Identifier 10.1109/JLT.2018.2885548

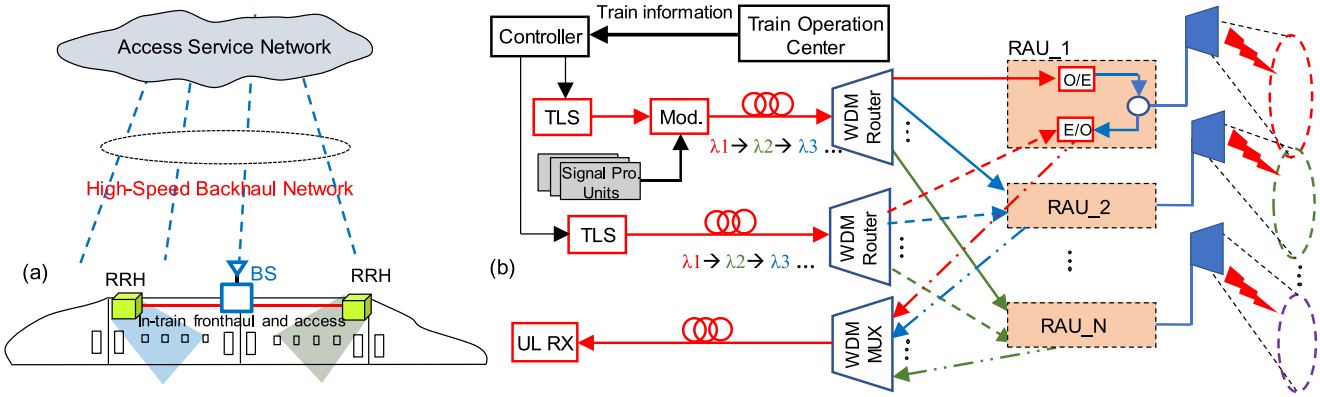

Fig. 1. (a) Concept of a cell-less network for HSTs; (b) A cell-less network for HSTs by a moving fiber–wireless backhaul system.

(WDM) RoF and mmWave system to overcome the limitations in current solutions [15], [16]. In our proposed system, RoF links are employed for radio signal transmission between a central station (CS) and remote antenna units (RAUs). The links help to significantly simplify antenna sites and increase the optical spectral efficiency compared to digital optical transmission methods. The key technologies to realize such a network include a fast radio-cell switching, cancellation of the interference between adjacent cells, and connection of the CS to many radio cells for realizing uninterrupted communications to HSTs.

In this study, we demonstrate an ultrafast and switchable WDM fiber–wireless system in the W band for high-speed and handover-free communications to HSTs. We successfully transmitted approximately 20-Gb/s signals from a CS to a base station (BS), which is assumed to be located on HSTs, through different switched fiber–wireless links in the 90-GHz band. An ultrafast radio-cell switching in less than 4 μs was experimentally confirmed in the downlink direction. We also successfully demonstrated the cancellation of the interference between the adjacent cells using a cell-coordination technique, i.e., the standard Alamouti diversity scheme. Moreover, the possibility of connecting the CS and BS through 50 switched fiber–wireless links was experimentally confirmed. In addition, we successfully transmitted approximately 10-Gb/s signals from HSTs to the CS over switched wireless–fiber links in the uplink direction. An ultra-short interruption time of approximately 3.5 μs was experimentally confirmed during radio-cell switching in the uplink direction, showing that an uninterrupted communication network can be realized. The possibility of connecting the BS to the CS through 80 switched wireless–fiber links was also successfully demonstrated.

This paper is an expanded version of our previous work [17]. Here, we further explain the system concept for transmissions in both downlink and uplink directions. We describe the details of the experimental setups and results. Moreover, we present the experimental results of the transmission over different fiber lengths using an optical local oscillator (LO) signal distributed from the CS. We also demonstrate the proof-of-concept and explain the details of the experimental setup and results of the uplink system, the summarized version of which is reported in [18]. The system link budget design for both downlink and uplink systems is also discussed. To the best of our knowledge, this study is the first to demonstrate the switched WDM fiber–wireless system for moving users with high capacity, a large number of connected radio cells, and ultrafast radio-cell switching. The remainder of the paper is organized as follows. Section II presents the concept of an uninterrupted communication network for HSTs in the downlink and uplink directions. Section III presents the proof-of-concept demonstration of high-speed and uninterrupted communications in the downlink direction from the CS to the BS on HSTs. In Section IV, we present the demonstration of the uplink system from the BS to the CS. Section V discusses the system link margin design and Section VI concludes the paper.

II. Concept of a Cell-Less Network for HSTs

The basic concept of the proposed cell-less network for HSTs is shown in Fig. 1(a). The idea is moving the BSs, which are located on the ground in conventional systems, to the trains such that users on the trains can communicate with the same BSs during the movement to prevent frequent handovers. An in-train network, which consists of a fronthaul and a radio-access network, can be optimized to provide maximized throughput and coverage to the users. In the proposed system, a moving backhaul network that connects the BSs on HSTs with an access-service network on the ground is of utmost importance to realize handover-free communications. In this study, we develop a high-speed moving-backhaul network using a switched WDM fiber–wireless system in the mmWave band (Fig. 1(b)). In the system, many RAUs can be installed along the railway tracks to communicate with the BSs via mmWave backhaul links. The frequency band for the backhaul system can be different from those in the radio access networks (RANs), including 5G mobile networks. Owing to the large bandwidths and low atmospheric attenuation, the mmWave link in the W-band (75–100 GHz) is a promising candidate for a large-capacity and long-distance backhaul system for HSTs. In the downlink direction, radio signals from the CS can be transmitted to the RAUs using a WDM RoF network. At the RAUs, the received RoF signals are directly up-converted to the mmWave signals and transmitted to the BSs without having to perform any other signal processing

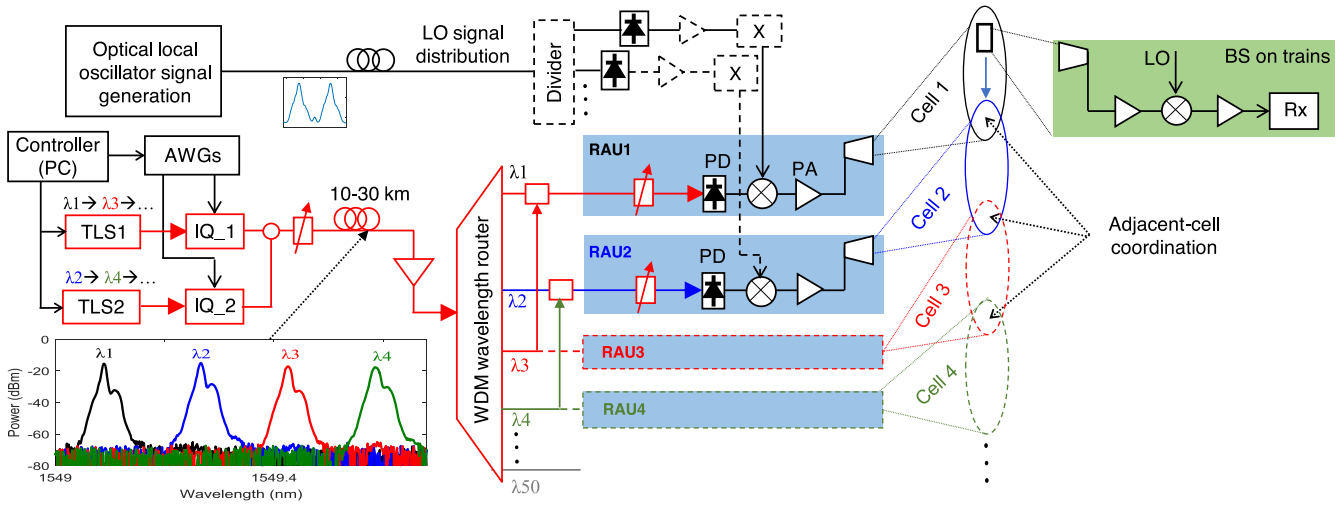

Fig. 2. Experimental setup for a handover-free communication to high-speed trains by switched WDM fiber–wireless system. Dashed-line parts were not performed in the proof-of-concept demonstration.

or conversions. When a train moves from one RAU to the coverage of the other, radio signals from the CS can be rerouted to the new RAU and a connection between the new RAU and the BS can be established. To achieve an uninterrupted communication between the trains and the access networks, the disconnect and connect procedures between the RAUs and the BSs should be established within a sufficiently short amount of time. The period during which the BSs receive no signals from the CS because of the RAU switching is called radio-cell switching. It should be less than a packet length to avoid the throughput drop during the train's movement. Different from other networks that implement radio-cell switching by sending and processing control signals, the switching procedure is executed by photonic technologies in the proposed system.

Unlike standard cellular networks, in the communication networks for HSTs, the train information, including location, velocity, and identified number of BSs, is available at the train operation centers. This information is very important and can be utilized to control and switch radio cells instead of using control signals as in cellular networks. In this network, a fixed wavelength can be assigned to each RAU for signal transmission from the CS. When the train moves to the coverage of one RAU, an optical switching technique can switch the optical signals to transmit radio signals to the RAU to which the train is approaching. This can be done precisely even before the train enters the coverage of the RAU using the train information from the train operation centers. Using this method, neither a separate control plane nor the use of uplink signal information is required for radio-cell switching, which can significantly reduce the complexity and the implementation time. Many optical-switching methods can be used for signal switching. In this study, we propose an ultrafast method using a wavelength-tunable laser (TLS) (Fig. 1(b)). In this method, optical signals from the TLS are modulated by radio signals at an optical modulator. The modulated optical signals are then transmitted to a WDM router located at a division point over a fiber link. The outputs of the WDM router, corresponding to different wavelengths, are connected to the RAUs through different fiber links, depending on the wavelength assignment. When the train moves from one RAU to a new one, the TLS can be controlled to switch the wavelength to the value that is assigned to the new RAU. Using this method, radio signals can be switched from the old to the new RAUs and the communication connectivity between the CS and the BSs can be continuously maintained.

In the uplink direction, a moving backhaul network can also be developed. To reduce system complexity, a separated optical network from those in the downlink direction should be deployed for the uplink signal transmission. A TLS can be located at the CS, transmitting optical carrier signals to the RAUs. A fixed wavelength can also be assigned to each RAU for the uplink signal transmission. The TLS is connected to a WDM router via a fiber link. The outputs of the WDM router are then connected to the RAUs by different fiber links, depending on the wavelength assignment. Radio signals from the BSs, after being received at the RAUs, can be transmitted to the CS via different RoF links. These RoF links can be connected to a WDM multiplexer and transmitted to the CS via the same fiber link. Similar to the downlink system, when the train moves from one RAU to the next, the TLS can be controlled to transmit an appropriate optical carrier signal to the RAU to which the train is approaching. Using this method, radio signals from the BSs can be continuously transmitted to the CS after being received by different RAUs. Owing to the ultrafast wavelength switching of the TLS, the interruption of the received signals at the CS during the RAU switching can be very small and an uninterrupted communication network can be developed. In this system, the same carrier frequency can be reused for all RAUs to increase radio spectral efficiency. For radio signal transmissions between the CS and RAUs, the use of the analog waveform transmission by RoF systems can significantly simplify the RAUs and increase the optical spectral efficiency compared to digital transmission methods. To prevent interference in mmWave links, different carrier frequencies should be used for the downlink and uplink directions. For the alignment of antennas, the coverage cell is

designed along the service (railway track); thus, the antennas at the RAUs can be directed along the railway track so that the transmitter and receiver antennas can be well aligned. In addition, high-gain antennas with large diameters and large beam sizes, such as Cassegrain antennas, can be used in practical systems for easy alignment and for increasing the transmission distance [19]. In Sections III and IV, we present different proof-of-concept demonstrations in the experiment room to confirm the operational principle of the proposed system.

III. Downlink System Demonstration

A. Experimental Setup

The experimental setup for the proof-of-concept demonstration of a high-speed and uninterrupted communication from a CS on the ground to a BS on HSTs using a switched WDM fiber–wireless backhaul network is shown in Fig. 2. In the system, an intermediate-frequency-radio-over-fiber (IFoF) method is used to transmit mmWave signals from the CS to RAUs owing to its high spectral efficiency and low fiber-dispersion effect. In this method, a fixed wavelength is assigned to each RAU. Electrical signals in a low intermediate-frequency (IF) band (7 GHz in our experiment) are generated at the CS and transmitted over fiber links to the RAUs. We used a TLS with ultrafast wavelength switching to generate optical signals. For data modulation, we employed an optical single-side band (SSB) modulation method using an optical IQ modulator to reduce the fiber-dispersion effect. The modulated optical signals were fed to a single-mode fiber (SMF), amplified using an optical amplifier (EDFA) and transmitted to a WDM router. We used a burst-mode EDFA to reduce the effects of optical surges because of wavelength switching of the TLS [20]. The outputs of the WDM router were connected to appropriate RAUs via different SMFs. At the RAUs, the received optical signals were converted back to the IF signals using photodetectors and up-converted to the mmWave signals at 95 GHz using electrical balanced mixers in the W band. Local oscillator (LO) signals for the signal up-conversion can be remotely distributed from the CS to the RAUs. A high-precision optical modulation technology [21] would be very useful for generating stable LO signals in high-frequency bands. The up-converted mmWave signals were amplified using W-band power amplifiers (PAs) before being emitted into free space using 23-dBi-gain horn antennas and transmitted to the BS via mmWave backhaul links. In practical systems, the BSs are located on HSTs. In our experiment, the mmWave links between the RAUs and the BS had a distance of approximately 2 m. At the BS, the mmWave signal was received using another 23-dBi-gain horn antenna, amplified using a low-noise amplifier (LNA) and down-converted to an IF band using an electrical coherent detection. The signal was amplified using another LNA, sent to a real-time oscilloscope, and finally demodulated offline.

In this experiment, we evaluated the system performance for two different cases. In the first case, we used one TLS for the generation and transmission of optical-carrier signals to RAUs. In this case, only one RAU is activated to transmit radio signals to the BS. The TLS can switch the wavelength to transmit signals to different RAUs. This can simulate the movement of the train along the railway track. The TLS used in our experiment was a widely tunable MG-Y branch laser [22] with a field-programmable gate array control circuit for generating and switching optical carrier signals and can be controlled using a personal computer. In the experiment, we modulated the generated optical signals from the TLS by a 6-GHz-bandwidth orthogonal frequency-division multiplexing (OFDM) signal centered at 7 GHz. The signal comprising 256, 512, and 1024 subcarriers, 5% of which at each edge were inactive, was generated by an arbitrary waveform generator (AWG). The 16-QAM data modulation is applied to each subcarrier, resulting in a gross data rate of 21.6 Gb/s. A cyclic prefix with a length of 12.5% of the symbol period is inserted to each symbol so that a net data rate of 19.2 Gb/s can be achieved. The corresponding subcarrier spacings are 23.4375 MHz, 11.71875 MHz, and 5.859375 MHz for the subcarrier numbers of 256, 512, and 1024, respectively. These spacings are much larger than the proposed subcarrier spacings in the next-generation mobile standards [23]. However, our system is proposed for the backhaul transmission to the BSs and is separated from the RANs. After being transmitted over the backhaul system, received signals can be processed at the BSs before being fed to the RANs inside the trains. Therefore, the parameters of the signals transmitted over the backhaul system can be different from those in the RANs.

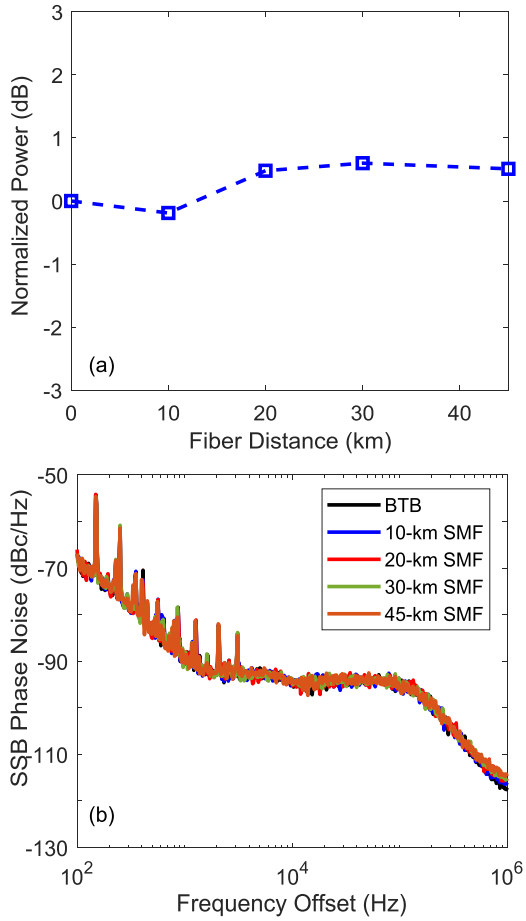

Fig. 3. (a) LO normalized power; and (b) SSB phase noise characteristics.

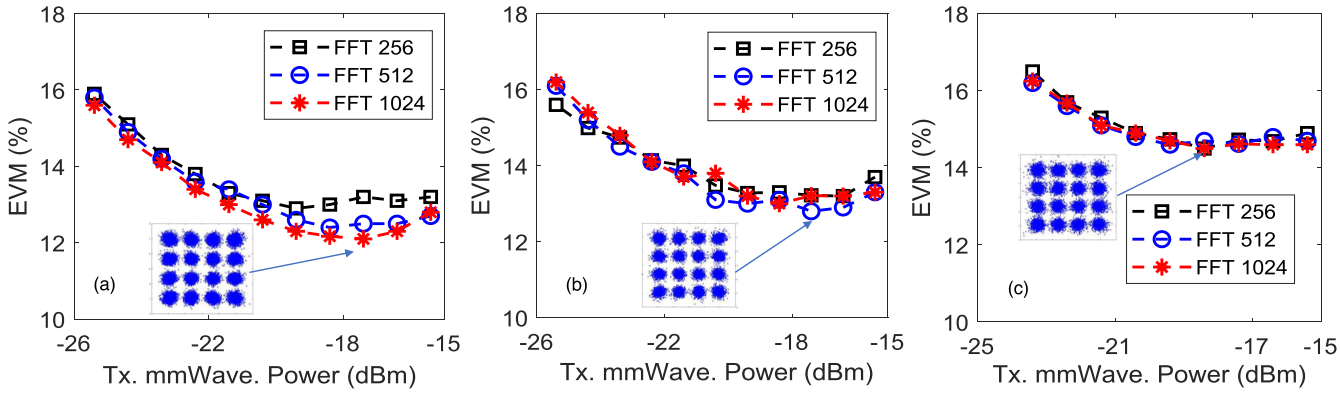

Fig. 4. Performance of OFDM signal for different FFT sizes and fiber transmission lengths: (a) 10-km SMF; (b) 20-km SMF; (c) 30-km SMF.

In the second case, we used two TLSs for generating optical signals at different wavelengths and transmitted them to two adjacent RAUs simultaneously. In this case, after being modulated by the OFDM signals at two optical IQ modulators, the optical signals were combined using a 3-dB optical coupler (OC) and transmitted to the WDM router via an SMF. We assumed that the first TLS generated odd-channel signals and the second TLS generated even-channel signals. To reduce the number of required wireless links, we routed the odd-channel signals from the outputs of the WDM router to the same RAU and the even-channel signals to another RAU. This does not affect the system performance evaluation compared to the case of using separated RAUs for different channels. Using the two-TLS scheme, an RAU is not required to switch to the next one, but to the cell after the next one in the same direction with the movement of the trains. The two adjacent RAUs simultaneously transmit mmWave signals to the BS. To handle the interference that can occur at the BS when the trains enter the overlapping coverage area of two adjacent cells, we proposed to coordinate the two cells using a standard 2×1 Alamouti space-time code [24]. This code allows the transmission of one spatial stream of information from two RAUs without causing interference and achieving full spatial diversity at the BS. The scheme can be easily applied to the OFDM signal on a subcarrier basis, assuming that the channel remains constant in time over two successive multicarrier symbols. The Alamouti scheme was applied to the system by transmitting two pre-coded signals to two adjacent RAUs that broadcast their respective signals to the BS. The receiver at the BS then jointly processed the two received signals and performed Alamouti decoding. In this experiment, the two coordinated OFDM signals were generated by two synchronized AWGs and had similar parameters with the OFDM signal used in the first case, except that the number of subcarriers was fixed to 512.

B. Experimental Results

We first evaluated the system performance for the first case. In this case, the LO signal for the signal up-conversion at the RAUs was generated at the CS and remotely distributed to the RAUs via a separated SMF. This can significantly simplify

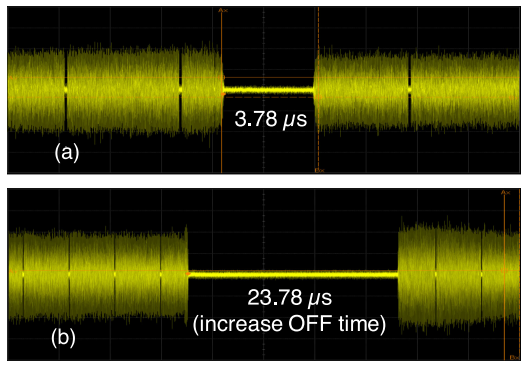

Fig. 5. Radio cell switching time by the wavelength-tunable laser: (a) off-time to a minimum value of 3 μs; (b) increase off-time to 20 μs.

the RAUs and help to reduce the cost, power consumption, and management complexity. It can also support the signal cooperation between adjacent cells by controlling the time delay and phase variations of the LO signals. In the experiment, we used a high-precision optical modulation technology for optical two-tone signal generation [21]. The generated optical signal was amplified using an EDFA at the CS and transmitted to the RAUs via an SMF. At the RAUs, the signal was up-converted to an mmWave LO signal at 90-GHz band using a high-speed photodetector. The signal was filtered using an electrical bandpass filter and amplified using a PA to drive the balanced mixers. For wireless systems in high-frequency bands, the quality of LO signals, including the phase noise and frequency stability, is very important to achieve satisfactory performance. We measured the power and the SSB phase noise of the generated LO signal at the RAU after being transmitted over different fiber cables. In this measurement, we used a 10-MHz-linewidth distributed-feedback laser for the optical LO signal generation. Fig. 3(a) shows the normalized power of the generated electrical LO signal at the RAU. The power is normalized to the power of the optical back-to-back transmission. A relatively constant power could be achieved, showing that the fiber-dispersion-induced power fading is negligible. Fig. 3(b) compares the phase-noise characteristics of the electrical LO signals. Owing to the phase correlation and frequency stability of the generated optical sidebands in our technology, the optical LO signals have a stable and

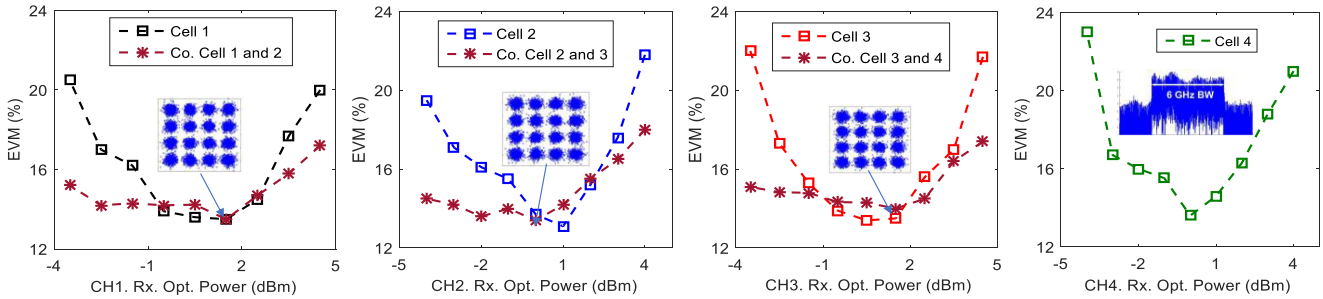

Fig. 6. Transmission performance of fiber–wireless links and joint coordination between adjacent cells.

low phase noise. As a result, the phase noise of the generated electrical LO signal is also very stable. In this case, the effect of fiber dispersion on the phase-correlated optical LO signal is negligible for transmission over several tens of kilometers of fiber. The measured results match the theoretical analysis in [25].

We evaluated the signal performance using the error vector magnitude (EVM) parameter. In practical systems, there may be multiple paths between the transmitters and the receivers. Differences in delays between the paths may cause destructive interference to the received signals. The delay spread is inversely proportional to the coherence bandwidth. In an OFDM system, the delay spread is an important parameter and the subcarrier spacing should be smaller than the coherence bandwidth [26]. The parameters of the OFDM signal, including subcarrier spacing, symbol length, and cyclic prefix length, should be carefully determined to reduce the effects of Doppler shifts and phase noise. In addition, fiber cables used to connect the CS with RAUs can have different lengths. Fig. 4 shows the OFDM signal performance for different subcarrier spacings after they were transmitted over the system with different fiber lengths. In this measurement, the cyclic prefix was fixed to one-eighth of the symbol period. All signal transmissions satisfy the EVM requirement for 16-QAM OFDM signals, which is approximately 14.84% for the bit error rate below the forward error correction limit of 2.2×10^{-3} [27]. However, the signal performance for the transmission over the 30-km-SMF system was relatively degraded because of the interaction between the phase noise of the tunable laser and the fiber dispersion effect [28]. Owing to the low phase noise of the LO signal, the signals using different subcarrier spacings had a similar performance. In systems with one TLS, radio-cell switching time is very important to realize uninterrupted communications to HSTs. In this case, the signal is switched from one RAU to the other by switching the wavelength of the TLS. We measured the interrupted time in the received signal at the BS when the TLS switched the wavelength. This was done by measuring the received IF signal at the BS in the time domain. Examples of the measurements are shown in Fig. 5. We observed a very fast cell switching (<4 μs), which includes 100-ns wavelength switching time, a minimum off-time of 3 μs of the TLS, and additional transmission delay over the system (Fig. (5a)). In this case, it is possible to set a guard time of the packets to less than 10 μs and the throughput of the packets cannot be degraded

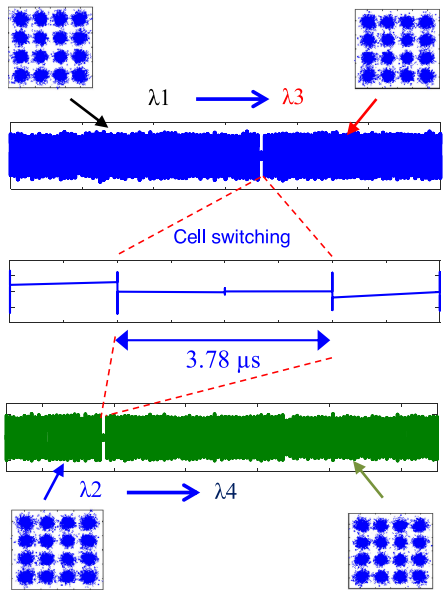

Fig. 7. Cell switching by the wavelength-tunable lasers.

by cell switching. An example of increasing the switching time by increasing the off-time of the TLS is shown in Fig. 5(b). In this example, an interrupted time of 23.78 μs was observed. With this switching time, a data packet can be lost during cell switching. Using other optical switching methods, such as active WDM switching, a low switching speed of several milliseconds is needed, thus, significantly limits the throughput of the networks.

We then investigated the performance in the second case using two TLSs for signal generation and transmission to two adjacent RAUs. We transmitted signals to four different RAUs and evaluated the signal performance. Because of the limitations of devices and the space in the experiment room, we combined the optical signals transmitted to RAU-1 and RAU-3 and the signals transmitted to RAU-2 and RAU-4 using 3-dB OCs. The optical signals transmitted to RAU-1 and RAU-3 and those to RAU-2 and RAU-4 were generated from the same TLS. Using this setup, we could evaluate the performance of four different switched fiber–wireless links using only two mmWave links. Fig. 6 shows the performance of the 16-QAM OFDM signals after they were transmitted over the systems for different received optical powers at the RAUs. We achieved satisfactory

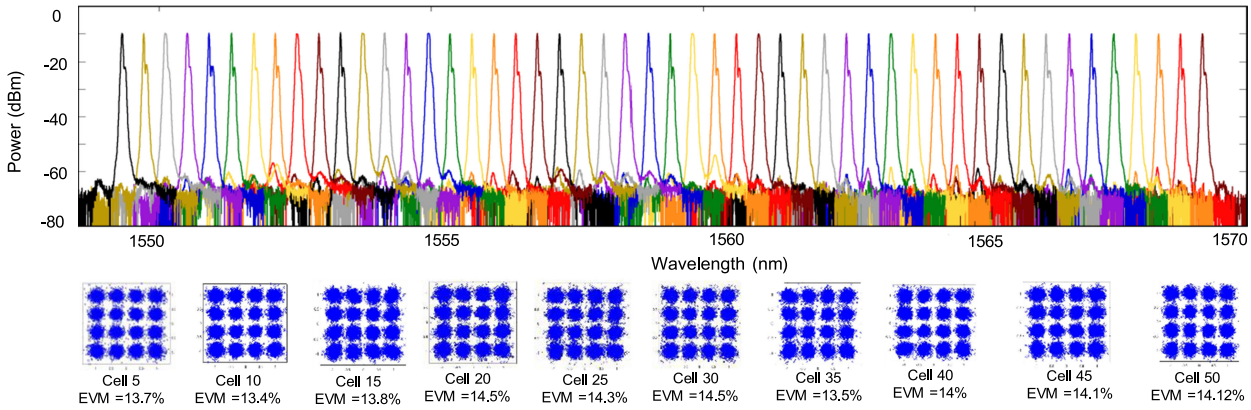

Fig. 8. Spectra of switched optical SSB signals and examples of signal performance at different cells.

performance for all signal transmissions with EVM values satisfying the 7% FEC performance requirement for 16-QAM signals. To cancel the interference in the received signal at the BS, we used a basic diversity transmission by a 2×1 Alamouti coding scheme. The performance for signal coordination between two adjacent cells is also shown in Fig. 6. We observed a higher performance than in the case of transmitting signals from a single cell, especially in low and high received power regions. The interference from the adjacent cells were successfully cancelled. Because of the lack of W-band attenuators at the time of the experiment, we could evaluate the signal performance and the transmission coordination for different received optical powers. However, the performance of different received optical powers at the RAUs represents the reduction in the received power at the BS and it is sufficient to evaluate the cell-coordination capability. For cell coordination to work properly, time delays between the two received signals should be optimized. In the system, fiber cables connecting the CS and RAUs can have different lengths. However, the information of fiber cables is available at the CS and a delay can be added to the signals before transmission to compensate for the delay difference. The LO signals used for signal up-conversions should have the same frequencies and phases. This can be easily achieved using centralized LO signal generation and transmission as shown in our system.

We evaluated the switching between cell 1 and cell 3, and cell 2 and cell 4, by recording the received signals at the receiver in the time domain. In this measurement, the first TLS was set to the auto-switching mode between $\lambda 1$ and $\lambda 3$ (switching between RAU-1 and RAU-3) and the second TLS was set to the auto-switching mode between $\lambda 2$ and $\lambda 4$ (between RAU-2 and RAU-4). Examples of the communication interruptions during cell switching are shown in Fig. 7. Similar to the first case, we observed an ultrafast cell switching of less than 4 μs. However, different from the first case, in the system using two TLSs, it may not be necessary to have a very fast cell switching because the adjacent RAUs are simultaneously activated to transmit signals to the trains. In the case that the cell size is longer than the length of the train, communication interruptions will not occur if the switching time is shorter than the time for the train to pass a cell. In this sense, a slow wavelength-tunable laser or other optical switching methods can be applied for cell switching. In our system, it is not necessary to lock the LO at the BSs with the LO at the transmitter. Instead, we use common phase carrier estimation to estimate the phase of the received signals by digital signal processing at the receiver. The phase noise is tracked using a blind decision directed algorithm. The main assumption of the algorithm is that the phase noise is changing slow enough so that its effect can be approximated as flat in frequency across all subcarriers and constant in time for the duration of the two OFDM symbols. After decoding at the receiver, the phase of the symbols is corrected using the previously estimated phase. The symbols are then estimated by direct decision. The current phase estimate can be updated by computing the angle between the demodulated symbols and the decoded symbols at each subcarrier and for two consecutive OFDM symbols on which the Alamouti scheme was applied.

The number of radio cells that can be connected and controlled by the same CS is very important to reduce the cost, management complexity, and especially the number of handovers due to the switch of CSs. The TLSs used in our experiment can generate and switch up to 100 different wavelengths. Half of the wavelengths may be used for uplink transmission and 50 wavelengths can be used for data transmission in the downlink. We investigated the possibility of connecting the system to 50 radio cells by measuring the performance of the switched fiber–wireless links using the wavelengths from the TLSs. Fig. 8 shows the optical spectra of the switched optical SSB signals measured at the input of the EDFA in Fig. 2. The modulated optical SSB signals were well maintained during wavelength switching, showing that the IF signals can be distributed properly to corresponding RAUs. We adjusted the bias controller of the IQ modulator every time the wavelength was switched to achieve the uniform optical spectra with relatively constant optical power at different wavelengths (Fig. 8). However, it is not necessary to have the same power level at different wavelengths to achieve satisfactory performance because the received optical power can vary. We then investigated the performance of the received signals after they were transmitted over the switched fiber–wireless links. The examples of the signal performance are shown in Fig. 8. In this measurement, we connected the optical signal from the TLS directly to the RAU without using the WDM

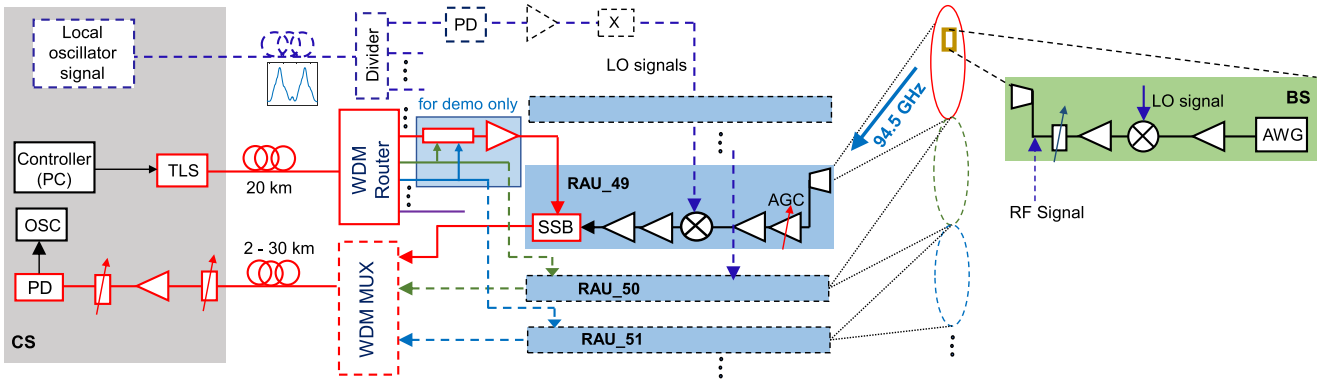

Fig. 9. Experimental setup for a proof-of-concept demonstration of uninterrupted communications from HSTs to the CS on the ground. Dashed-line parts were not performed in our proof-of-concept demonstration.

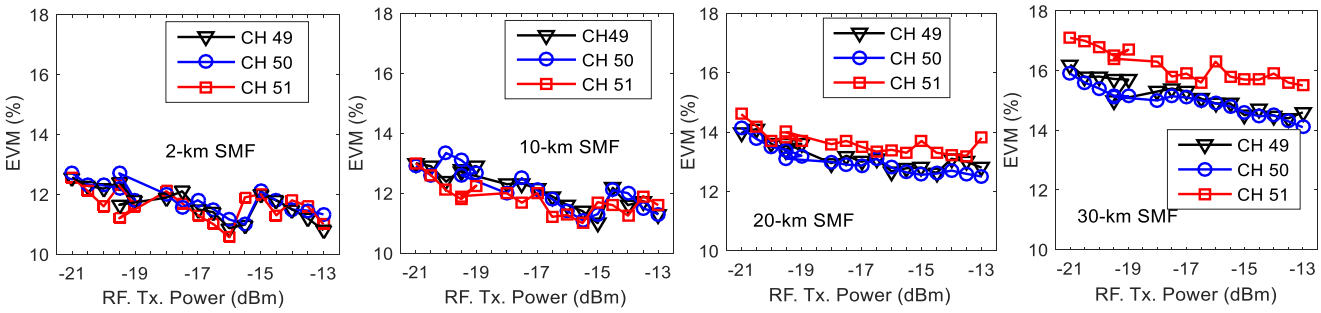

Fig. 10. Uplink signal performance for different RF transmit powers and different fiber lengths.

router. All the measurements for different fiber–wireless links were measured using the same RAU. We observed satisfactory performance for all signal transmissions. This confirms that a high-speed communication of more than 20 Gb/s gross-rate can be distributed from the CS to 50 RAUs and consequently transmitted to the BS on the trains without any signal interruptions. In other words, uninterrupted communications to HSTs can be achieved when the trains move inside the coverage of 50 RAUs, which can reach several tens of kilometers.

IV. Uplink System Demonstration

A. Experimental Setup

The experimental setup for the proof-of-concept demonstration of an uninterrupted communication from an HST to a CS using a switched WDM fiber–wireless system in the uplink direction is shown in Fig. 9. At the BS, which is assumed to be located on the trains, a 3-GHz-bandwidth OFDM signal at 7 GHz was generated using an AWG. The signal comprises 512 subcarriers, 5% of which at each edge were inactive. By loading 16-QAM data to each subcarrier, a gross data rate of 10.8 Gb/s can be obtained for uplink transmission. A cyclic prefix with the length of the one-eighth of the symbol period is inserted to each symbol, resulting in a net data rate of 9.6 Gb/s. The signal was amplified using a driver amplifier and up-converted to 94.5 GHz using an electrical mixer. The up-converted signal was amplified using a PA and emitted into free space using a 23-dBi-gain horn antenna. After being transmitted over approximately 1.5 m in free space, the signal was received using another 23-dBi-gain horn antenna at an RAU. At the RAU, the received mmWave signal was amplified using an LNA with which the gain can be controlled depending on the input power of the received signals. The use of the gain-controlled amplifier stabilizes the received signal power before the signal is transmitted to the CS via the optical network. This is to prevent the performance degradation that may be caused by the limited dynamic range of analog RoF systems. In practical systems, the gains of the amplifiers can be controlled by controlling the information from the CS. In the proposed system, because the locations of the trains can be precisely determined at the CS, the received power levels at the RAUs can also be predicted. Consequently, appropriate values can be set for the gains of the amplifiers, depending on the positions of the trains. In general, it is not required to change the amplifiers' gains instantaneously with the movement of the trains. Alternatively, the gains can be adjusted in every specific power range of the received signals and the control of the amplifiers from the CSs can be performed more easily.

In our experiment, to simulate the use of the variable-gain amplifier, we used a variable attenuator to adjust the received power of the mmWave signal before feeding it to the LNA at the RAU. The amplified signal is down-converted to an IF band and amplified by another LNA. The signal was then amplified using a driver amplifier before being fed to an IFoF link and transmitted to the CS. For the generation of optical-carrier signals for the IFoF links, we used a TLS located at the CS and transmitted the generated signals to the RAUs. In this experiment, the TLS was

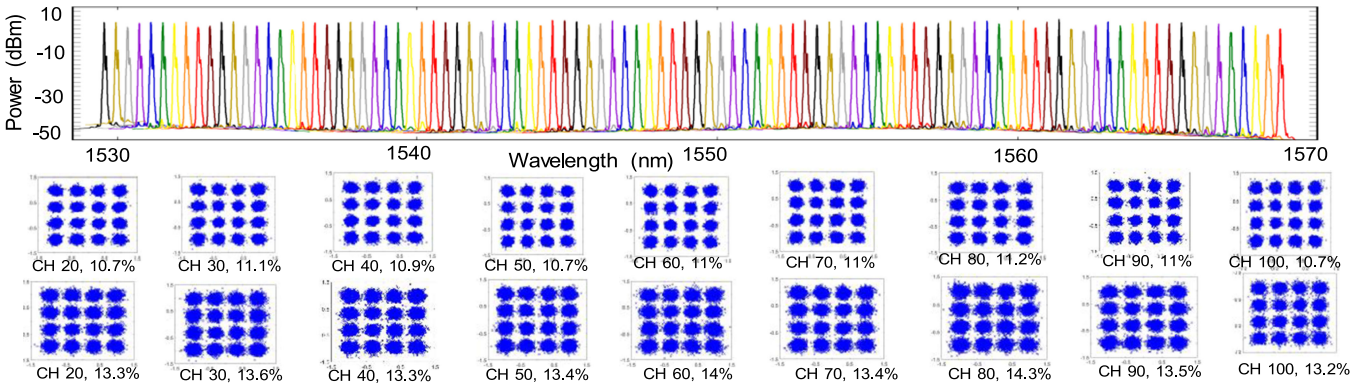

Fig. 11. Spectra of the switched optical SSB signals and examples of the signal performance for systems using 10-km SMF (upper) and 20-km SMF (lower).

connected to a WDM router via a 20-km SMF. The outputs of the WDM router were connected to the RAUs using different SMFs. For simplicity, a fixed wavelength was assigned to each RAU. In practical systems, when a train moves closely to an RAU, the TLS can be controlled to transmit an appropriate optical-carrier signal to the RAU for carrying the received radio signal to the CS using the train information from the train operation centers. At the RAU, the switched optical carrier signal was modulated by the down-converted IF signal and transmitted back to the CS. To reduce the number of SMFs, a WDM MUX can be used to combine the modulated optical signals from different RAUs. The combined signal can be transmitted to the CS through the same fiber link. In our demonstration, to simulate the movement of the train and the switch of the RAUs, we combined three optical signals, which correspond to channel numbers 49, 50, and 51 of the TLS, from the outputs of the WDM router using 3-dB OCs. We then connected the combined signal to a fixed RAU for carrying the received radio signals to the CS. Using this scheme, we investigated the switch of the RAUs by switching the optical-carrier signals and evaluated the performance of switched wireless–fiber links. The WDM MUX was not required in this demonstration. For data modulation at the RAU, similar to the downlink system, we used an optical IQ modulator to generate an optical SSB signal. The modulated signal was transmitted to the CS via an SMF. To investigate the performance for different cases, we inserted an optical amplifier (EDFA) and variable optical attenuators to the optical link. At the CS, the signal was converted back to the electrical signals, sent to a real-time oscilloscope, and finally demodulated offline. The LO signals for signal down-conversions at the RAUs can be remotely distributed from the CS. For simplicity, we used an LO signal at 85 GHz from an electrical synthesizer in this experiment.

B. Experimental Results

In the uplink system, the performance for different received powers relates to the movement of the trains to the RAUs. In general, analog RoF systems have a relatively limited dynamic range of the input radio signal power. First, we evaluated the system performance for different transmit powers of the mmWave signal. The signal performance of the 94.5-GHz signal after being transmitted over switched wireless–fiber links for different transmit powers is shown in Fig. 10. We observed a very satisfactory performance for transmissions over 2-km, 10-km, and 20-km SMF systems for the 16-QAM OFDM signal. For the transmission over the 30-km SMF system, the performance was relatively degraded because of the interaction of the phase noise of the tunable laser with the fiber dispersion. The conversion of large phase noise of the optical carrier signals to intensity noise due to fiber dispersion increases with the fiber length, resulting in performance degradation [28]. This happens even for the systems that use an optical SSB modulation for OFDM signal transmission. However, an SMF with the length of 30 km would be sufficiently long for connecting a CS with RAUs because the distance between CSs would be approximately 50 km in practical systems [16]. The performance of channel 51 was relatively degraded compared to other channels for the 20-km and 30-km SMF transmission. This can be caused by the larger phase noise of the optical carrier signal at this wavelength due to the imperfection of the tunable laser. After a short fiber transmission, the interaction of the optical signal phase noise with fiber dispersion is not significant. However, after a long fiber transmission, the effect of fiber dispersion and its interaction with the phase noise become larger, resulting in the signal performance degradation. We observed that the performance was relatively stable over a wide range of the transmit powers because the received power levels were adjusted before the signals were transmitted over the fiber links. In this measurement, we set the variable electrical attenuator at the RAU to a large value for high received power levels and gradually reduced the attenuation for low received power levels. With this adjustment, the received mmWave signals at the RAU can be maintained within the limited dynamic range of the IFoF systems. Slight variations in the EVM performance (Fig. 10) occurred because the adjustment of the attenuator was not fully optimized for all values of the received powers. In practical systems, using a careful link design, an optimized adjustment of the attenuator can be performed to achieve a smooth performance for different received signal powers. A transmit power of approximately -20 dBm at the input of the transmit antenna at the BS, which corresponds to a received power of approximately -50 dBm at the output of the receive antenna at the RAU, should be

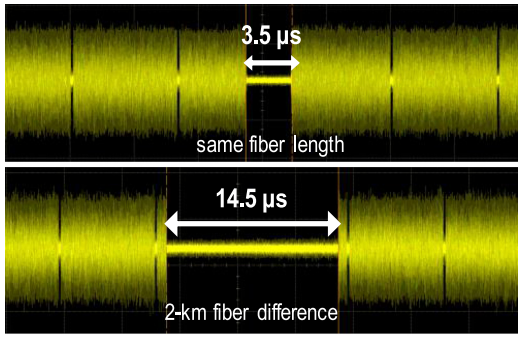

Fig. 12. The interrupted time during radio cell switching.

received to successfully demodulate the transmitted signals. This observation is very important to estimate the maximum cell size of the RAUs and design the system link budget, which is discussed in Section V. The minimum required received power is dependent on the lengths of the SMFs of the IFoF systems. Thus, a joint optimization of the IFoF systems and the cell size of the RAUs should be considered to enhance the signal performance.

Increasing the number of RAUs that can be connected and controlled by the same CS is very important in the proposed system. The TLS used in our experiment can generate up to 100 wavelengths. We measured the optical spectra of the modulated optical SSB signals and the results are shown in Fig. 11. In this measurement, we connected the TLS directly to the RAU without using the WDM router. The optical spectra were measured before photodetection at the CS. We observed that the modulated optical SSB signal was well maintained during wavelength switching. Examples of the signal performance after transmission over different switched wireless–fiber links in the uplink direction are also shown in Fig. 11. These results were measured for the transmission over the systems using 10-km SMFs (upper) and 20-km SMFs (lower). We showed satisfactory system performance for all signal transmissions using optical channels from 20 to 100, which correspond to the wavelengths from 1529.55 nm to 1561.41 nm. For large-wavelength channels from 1561.82 nm to 1569.18 nm, the performance was relatively degraded because of the limited operational wavelength range of the optical amplifier used in the experiment.

Similar to the downlink system, the switching time of the RAUs is important to achieve an uninterrupted communication to HSTs. In the proposed system, the switching of the RAUs is performed at the CS by the TLS. We measured the interruption time during RAU switching by monitoring the received signals at the CS in the time domain. In this proof-of-concept demonstration, we simulated the movement of the train and the switching of the RAUs by switching the wavelengths of the TLS. Fig. 12 shows the measured results for two different cases: (1) using fiber cables with the same length, and (2) using fiber cables with a 2-km-length difference, for connecting the two RAUs with the CS. In the second case, we used fiber cables with a 2-km-length difference to connect the two outputs of the WDM router to the 3-dB OC. In the first case, we observed an ultrafast switching time of approximately 3.5 μs, which consists of 100-ns wavelength switching, 3-μs minimum off-time of the TLS, and additional transmission delay. In the second case, the switching time increased to approximately 14.5 μs. This is different from the downlink system and the use of the SMFs with different lengths caused additional delay. Fiber cables used to connect any two adjacent RAUs with the CS should be optimized to prevent signal interruptions at the CS. For instance, a maximum fiber-length difference of approximately 1.2 km should be used to keep a packet guard time of less than 10 μs to prevent the throughput reduction during radio-cell switching. The measured results show an ultrafast switching between the adjacent radio cells and confirm that the proposed system can provide an uninterrupted communication from HSTs to the access networks on the ground. Using the proposed system, the radio spectral efficiency can be significantly increased because the same radio frequency can be reused in all RAUs. It also helps to eliminate the interference from the adjacent cells because only one RAU is activated at a time. Similar to the downlink system, to reduce the requirement on the switching time of the TLS, two TLSs can be used to transmit optical-carrier signals to adjacent RAUs. In this case, two adjacent RAUs can be activated at the same time to receive signals from the trains. When the train moves to the overlapping area of two RAUs, the interference may occur at the CS. A standard 2×1 receiver diversity scheme, such as maximum ratio combining, can be applied at the CS to constructively combine the received signals and avoid destructive interference.

V. System Link-Budget Design

The link-budget design is important for cell planning and should consider all gain and loss factors. The gain factors include the gains of the power amplifier at the transmitter and the LNA at the receiver and the gains of the transceiver antennas. The loss factors include free space, atmospheric, and rain losses. The received power after being transmitted over an mmWave link can be calculated by

$$P_R = P_T + G_T + G_R - 20 \times \log_{10}\left(\frac{4.\pi.d.f}{c}\right) - (A+R) \times d - M, \quad (1)$$

where G_T and G_R are the transmitter and receiver antenna gains, respectively, *A* and *R* are the atmospheric and rain attenuations, respectively, P_T is the transmit power incident to the transmit antenna, *d* is the mmWave transmission distance, *f* is the frequency of the mmWave signal, and *M* is the link margin for other effects such as fading and fog attenuations. Atmospheric attenuation *A* at the frequency of the 90-GHz band is approximately 1 dB/km. In (1), we assume that the free space loss for the mmWave signal follows the Friis equation [29]. There have been no studies on path loss models and measurements of mmWave signals in the 90-GHz band. We performed a simple measurement to confirm the applicability of the Friis equation for radio links in the 90-GHz band. The measured results and the comparisons with the Friis equation are shown in Fig. 13. In this measurement, we generated and transmitted a carrier signal at 92 GHz and measured the received power by a spectrum analyzer. A 3-dBi-gain omni antenna was used at the transmit-

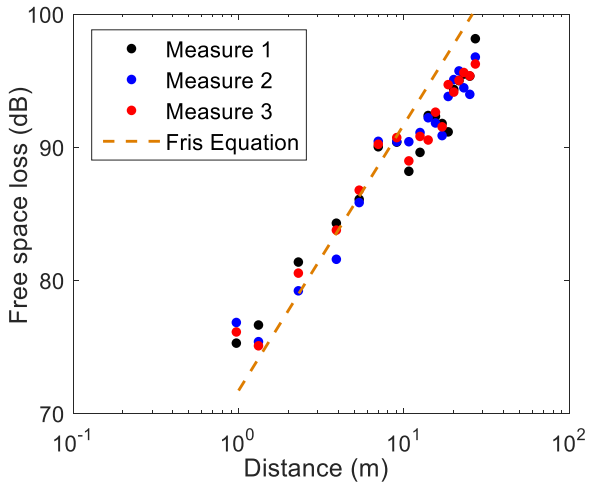

Fig. 13. Free-space loss measurement for a carrier signal at 92 GHz.

TABLE I
SYSTEM LINK BUDGET DESIGN

Parameters	Downlink	Uplink
Transmit power	20 [dBm]	20 [dBm]
Transceiver antenna gain	50 [dBi]	50 [dBi]
Signal bandwidth	6 [GHz]	3 [GHz]
Modulation format	16 QAM	16 QAM
Maximum cell size	1.0 [km]	1.0 [km]
Atmospheric attenuation	1 [dB/km]	1 [dB/km]
Rain attenuation	23.2 [dB/km]	23.2 [dB/km]
Free space loss	131.7 [dB/km]	131.7 [dB/km]
Received power	-35.9 [dBm]	-35.9 [dBm]
Sensitivity	-45 [dBm]	-50 [dBm]
Link margin	9.1 [dB]	14.1 [dB]

ter and a horn antenna with a gain of 23 dBi was used at the receiver. The reason for using the 3-dBi-gain omni antenna at the transmitter is to avoid the measurement inaccuracy that might be caused by the unintentional misalignment between the transmitter and receiver antennas. The measurement was conducted on a straight street under a sunny weather. The measured results fitted the theoretical estimation by the Friis equation well (Fig. 13). Measurement considering multipath-fading and other effects should be conducted to achieve a more precise model for mmWave links. However, for the purpose of link budget design, the data shown in Fig. 13 is sufficient for path loss estimation. The free-space loss is not dependent on the gains of antennas. Therefore, after confirming the possibility of using the Friis equation for free-space loss at the 90-GHz band using small-gain antennas, we can apply the equation for the estimation of the maximum cell size using high-gain antennas.

Rain attenuation can be estimated with the following equation based on the rainfall rate parameter [30]

$$R\,[dB/km] = k \times r^{\alpha} \tag{2}$$

where r (mm/h) is the rain intensity and coefficients k and α are frequency-dependent and can be determined using curve-fitting equations or a set of specified values given in Recommendation P.838-2 [31]. In the link budget design, the operational availability due to rain attenuation is an important parameter. For mobile backhaul links for HSTs, an availability of approximately 99.99% may be required. The system availability can be estimated using the statistical rainfall data over a long period of time and a specific rainfall rate can be defined for each required availability ratio [30]. Based on the determined rainfall rate, the rain attenuation can be calculated using (2). For example, with an availability requirement of 99.99%, a rainfall rate of 63 mm/h, corresponding to an attenuation of 23.2 dB/km, should be considered for the system to operate in Japan [32].

Table I shows an example of the link budget design for the mmWave system in both downlink and uplink directions. In this example, we calculated the link budget for an open-space environment and assumed that the maximum transmission distance is 1 km. The received power was calculated by summing the gain factors and subtracting the loss factors. The receiver sensitivity is based on the measurement results shown in Figs. 4 and 10. In the proof-of-concept experiments, the small-gain (23-dBi-gain) horn antennas were used because of the limited space in the experiment room. For a real-world implementation, high-gain antennas should be used to increase the cell size [33]. Here, the determined receiver sensitivity derived from the proof-of-concept experiment can be used as a reference value for the estimation of the maximum wireless link distance. In practice, when increasing the transmission distance using high-gain antennas, the required receiver sensitivity might be different because of the additional transmission influences, such as multipath fading and vibrations. In addition, due to the trains' vibrations during the movement, the antenna direction might be deviated from the maximum direction. In this case, a loss margin might be needed to compensate for the misalignment, and it can be included in the total link margin shown in Table I. Furthermore, because of the narrow beamwidth of the mmWave signals and the installation position of antenna sites, the railway track area close to an antenna site might not be covered by radio signals from that antenna. In this case, radio cells should be organized such that the undetectable areas can be covered by adjacent radio cells. In other words, there are overlapping coverage areas between the radio cells. In addition, owing to mechanical reason, the maximum direction of the downlink antennas might not be directed parallelly to the railway track. Considering these facts, the maximum coverage size of a radio cell might be smaller than the estimated maximum transmission distance of the mmWave link. To maximize the coverage area of the radio cells, antennas with special radiation patterns should be designed to direct the maximum radiation direction along the railway track. On the other hand, in practical systems, power consumption of RAUs is an important factor and should be optimized to reduce the operation cost. The power consumption of the RAUs is exponentially proportional to the output power of the PAs at the RAUs. Therefore, the transmit powers from the RAUs should be optimized to reduce the system power consumption [34]. For transmission inside tunnels, radio signals experience a lower attenuation than the path loss in the open

space [35]. This relates to the tunnel geometry, electromagnetic properties of the wall inside the tunnel, and the frequency. Thus, the link-budget design should be calculated case by case, depending on the tunnel characteristics.

Besides the link-budget design, the Doppler effect is another important parameter in studying the communications to HSTs. The Doppler frequency shift is inversely proportional to the channel coherence time, which is a measure of channel variation over time. The maximum Doppler shift is

$$f_{\max} = f \times \frac{v}{c} \tag{3}$$

where f is the carrier frequency of the mmWave links in Hz, v is the relative speed of the trains, and c is the speed of light. If a train moves at a speed of 500 km/h and the frequency of the mmWave links is 92 GHz, a maximum Doppler shift of 42.6 kHz can be estimated. The estimated Doppler shift is relatively small with respect to the carrier frequency. It can be compensated using digital signal processing at the receivers. In communication networks for HSTs, the frequency and velocity of the trains are well known. Thus, real-time recorded data can be used to shift the frequency of received signals by an offset inversely to the Doppler shift such that the received signals can be located at the accurate frequency for proper signal demodulation. In the downlink system, the receivers are located at the BS; thus, relatively complicated digital signal processing can be employed at the receivers to compensate for the Doppler shift and other transmission impairments before the signals are transmitted to end users. Moreover, since the train position and Doppler shifts are known at the CS, this can also be done before transmission by digital preprocessing. In the uplink system, receivers are located at the CS and the received signals can be processed to eliminate the Doppler effects and other transmission impairments.

VI. Conclusion

This study demonstrated a high-speed and handover-free communication network for high-speed trains using a switched wavelength-division multiplexing fiber–wireless system in the W band. We successfully transmitted approximately 20-Gb/s and 10-Gb/s signals over the switched fiber–wireless links in the downlink and uplink directions, respectively. An ultrafast radio-cell switching of less than 4 μs was experimentally confirmed for both downlink and uplink systems, which is sufficiently small to avoid the throughput drop and communication interruptions during radio cell switching. By activating many radio cells simultaneously, the interruption time can be further reduced or eliminated. We also successfully demonstrated the cell coordination and the interference cancellation between adjacent cells using a basic transmission diversity by the Alamouti coding scheme. The possibility of connecting a central station with many radio cells was experimentally investigated. The results showed that a handover-free communication network of up to several tens of kilometers can be achieved for high-speed trains. The proposed system will provide high-speed and advanced services to fast-moving users on high-speed trains in future 5G and beyond networks.

References

[1] L. Wang, T. Han, Q. Li, J. Yan, X. Liu, and D. Deng, "Cell-less communications in 5G vehicular networks based on vehicle-installed access points," *IEEE Wireless Mag.*, vol. 24, no. 6, pp. 64–71, Dec. 2017.

[2] F. Hasegawa *et al.*, "High-speed train communications standardization in 3GPP 5G NR," *IEEE Commun. Stand. Mag.*, vol. 2, no. 1, pp. 44–52, Mar. 2018.

[3] *Study on Scenarios and Requirements for Next Generation Access Technologies*, 3GPP, TR 38.913 (V14.2.0), Mar. 2017.

[4] *Introduction to Railway Communication Systems*, Report ITU-R M.2395-0, Nov. 2016.

[5] 3GPP, "Technical specification group radio access network; Mobile relay for evolved universal terrestrial radio access (E-UTRA)," 3GPP, Tech. Rep. TR 36.836, Nov. 20, 2012.

[6] Y. Sui, J. Vihriala, A. Papadogiannis, M. Sternad, W. Yang, and T. Svensson, "Moving cells: A promising solution to boost performance for vehicular users," *IEEE Commun. Mag.*, vol. 51, no. 6, pp. 62–68, Jun. 2013.

[7] S. Mumtaz, J. M. Jornet, J. Aulin, W. H. Gerstacker, X. Dong, and B. Ai, "Terahertz communication for vehicular networks," *IEEE Trans. Veh. Technol.*, vol. 66, no. 7, pp. 5617–5625, Jul. 2017.

[8] C. Wang, A. Ghazal, B. Ai, Y. Liu, and P. Fan, "Channel measurements and models for high-speed train communication systems: A survey," *IEEE Commun. Surv. Tuts.*, vol. 18, no. 2, pp. 974–987, second quarter 2016.

[9] S. Buzzi and C. D'Andrea, "Cell-free massive MIMO: User-centric approach," *IEEE Wireless Commun. Lett.*, vol. 6, no. 6, pp. 706–709, Dec. 2017.

[10] T. Kawanishi, A. Kanno, and H. S. C. Freire, "Wired and wireless links to bridge networks: Seamlessly connecting radio and optical technologies for 5G networks," *IEEE Microw. Mag.*, vol. 19, no. 3, pp. 102–111, May 2018.

[11] B. Lannoo, D. Colle, M. Pickavet, and P. Demeester, "Radio-over-fiber-based solution to provide broadband internet access to train passengers," *IEEE Commun. Mag.*, vol. 45, no. 2, pp. 56–62, Feb. 2007.

[12] J. Wang, H. Zhu, and N. J. Gomes, "Distributed antenna systems for mobile communications in high speed trains," *IEEE J. Sel. Area Commun.*, vol. 30, no. 4, pp. 675–683, May 2012.

[13] Y.-T. Hsueh *et al.*, "A novel wireless over fiber access architecture employing moving chain cells and RoF technique for broadband wireless applications on the train environment," in *Proc. Opt. Fiber Commun. Conf.*, 2011, Paper no. OWT3.

[14] C. Yeh *et al.*, "Theory and technology for standard WiMAX over fiber in high speed train systems," *J. Lightw. Technol.*, vol. 28, no. 16, pp. 2327–2336, Aug. 2010.

[15] P. T. Dat, A. Kanno, N. Yamamoto, and T. Kawanishi, "WDM RoF-MMW and linearly located distributed antenna system for future high-speed railway communications," *IEEE Commun. Mag.*, vol. 53, no. 10, pp. 86–94, Oct. 2015.

[16] A. Kanno, P. T. Dat, N. Yamamoto, and T. Kawanishi, "Millimeter-wave radio-over-fiber network for linear cell systems," *J. Lightw. Technol.*, vol. 36, no. 2, pp. 533–540, Jan. 2018.

[17] P. T. Dat *et al.*, "High-speed and handover-free communications for high-speed trains using switched WDM fiber–wireless system," in *Proc. Opt. Fiber Commun. Conf.*, 2018, Paper no. Th4D.2.

[18] P. T. Dat *et al.*, "Cell-less network for handover-free communications to high-speed trains using a switched WDM fiber–wireless backhaul," in *Proc. Eur. Conf. Opt. Conf.*, 2018, Paper no. Th1B.6.

[19] T. Hattori *et al.*, "Study of a millimeter wave communications system for railway trains," *JR East Tech. Rev.*, no. 33, pp. 37–42, 2015.

[20] M Shiraiwa *et al.*, "New burst-mode erbium-doped fiber amplifier with wide linearity and high output power for uplink analog radio-over-fiber signal transmission," *IEICE Trans. Electron.*, vol. 98, no. 8, pp. 832–839, Aug. 2015.

[21] A. Kanno *et al.*, "Coherent radio-over-fiber and millimeter-wave radio seamless transmission system for resilient access networks," *IEEE Photon. J.*, vol. 4, no. 6, pp. 2196–204, Dec. 2012.

[22] Y.-K. Yeo *et al.*, "A 448 $\times$ 448 optical cross-connect for high-performance computers and multi-terabit/s routers," in *Proc. Opt. Fiber Commun. Conf.*, 2010, Paper no. OMP6.

[23] A. Zaidi, R. Baldemair, V. Moles-Cases, N. He, K. Werner, and A. Cedergren, "OFDM numerology design for 5G new radio to support IoT, eMBB, and MBSFN," *IEEE Commun. Stand. Mag.*, vol. 2, no. 2, pp. 78–83, Jun. 2018.

[24] M. Alamouti, "A simple transmit diversity technique for wireless communications," *IEEE J. Sel. Areas Commun.*, vol. 16, no. 8, pp. 1451–1458, Oct. 1998.

[25] R. Hofstetter, H. Schmuck, and R. Heidemann, "Dispersion effects in optical millimeter-wave systems using self-heterodyne method for transport and generation," *IEEE Trans. Microw. Theory Techn.*, vol. 43, no. 9, pp. 2263–2269, Sep. 1995.
[26] W-W. Choi *et al.*, "Mobile hotspot network system for high-speed railway communications using millimeter waves," *ETRI J.*, vol. 38, no. 6, pp. 1052–1063, Dec. 2016.
[27] T. L. Thanh, V. N. Q. Bao, P. T. Dat, A. Kanno, and T. Kawanishi, "10-Gb/s wireless signal transmission over a seamless IM/DD fiber-MMW system at 92.5 GHz," in *Proc. IEEE Int. Conf. Commun.*, 2015, pp. 1364–1369.
[28] S. Yamamoto, N. Edagawa, H. Taga, Y. Yoshida, and H. Wakabayashi, "Analysis of laser phase noise to intensity noise conversion by chromatic dispersion in intensity modulation and direct detection optical-fiber transmission," *J. Lightw. Technol.*, vol. 8, no. 11, pp. 1716–1722, Nov. 1990.
[29] H. Friss, "A note on a simple transmission formula," *Proc. IRE*, vol. 34, no. 5, pp. 254–256, May 1946.
[30] *Specific Attenuation Model for Rain for Use in Prediction Methods*, ITU-R P.838–2 Recommendation, 2003.
[31] P. T. Dat, A. Kanno, K. Inagaki, and T. Kawanishi, "High-capacity wireless backhaul network using seamless convergence of radio-over-fiber and 90-GHz millimeter-wave," *J. Lightw. Technol.*, vol. 32, no. 20, pp. 3910–3923, Oct. 2014.
[32] A. Hirata *et al.*, "120-GHz-band millimeter-wave photonic wireless link for 10-Gb/s data transmission," *IEEE Trans Microw. Theory Techn.*, vol. 54, no. 5, pp. 1937–1944, May 2006.
[33] A. Kanno *et al.*, "20-Gbaud QPSK optical and radio transmission using high-gain antennas for resilient access networks," in *Proc. IEEE Summer Top. Meetings*, 2012, pp. 145–146.
[34] P. T. Dat *et al.*, "Energy and deployment efficiency of a millimeter-wave radio-on-radio-over-fiber system for railways," in *Proc. Opt. Fiber Commun. Conf.*, 2013, Paper no. JTh2A.61.
[35] A. Hrovat, G. Kandus, and T. Javornik, "A survey of radio propagation modeling for tunnels," *IEEE Commun. Surv. Tuts.*, vol. 16, no. 2, pp. 658–669, Aug. 2014.

Pham Tien Dat (M'12) received the B.Eng. degree in electronics and telecommunication engineering from the Posts and Telecommunications Institute of Technology, Vietnam, in 2003, and the M.Sc. and Ph.D. degrees in science of global information and telecommunication studies from Waseda University, Japan, in 2008 and 2011, respectively. In 2011, he joined the National Institute of Information and Communications Technology, Japan. His research interests are in the field of microwave/millimeter-wave photonics, radio-over-fiber, and optical wireless systems.

Atsushi Kanno (M'11) received the B.S., M.S., and Ph.D. degrees in science from the University of Tsukuba, Japan, in 1999, 2001, and 2005, respectively. In 2005, he was with the Venture Business Laboratory of the Institute of Science and Engineering, University of Tsukuba. In 2006, he joined the National Institute of Information and Communications Technology Japan. His research interests are microwave/millimeter-wave/terahertz photonics, ultrafast optical communication systems, and lithium niobate optical modulators.

Dr. Kanno is a Member of the Institute of Electronics, Information and Communication Engineers and the Japan Society of Applied Physics.

Keizo Inagaki received the B.E. and M.E. degrees in electrical engineering from Kyoto University in 1985 and 1987, respectively, and D.E. degree from the Tokyo Institute of Technology in 2011. In 1987, he joined ATR Optical and Radio Communications Research Laboratories, where he was involved in the research and development of free space laser communication systems. In April 2002, he moved to ATR Wave Engineering Laboratories, where he joined the research project on optical gyroscope. Since December 2009, he has been with the National Institute of Information and Communications Technology, Japan, where he is involved in the research and development of high-precision measurement using advanced photonics technologies.

Mr. Inagaki is a Member of the Institute of Electronics, Information and Communication Engineers.

François Rottenberg (M'18) received the M.Sc. degree (highest distinction) in electrical engineering from the Université catholique de Louvain (UCL), Louvain-la-Neuve, Belgium, in 2014, and the Ph.D. degree jointly from UCL and Université libre de Bruxelles (ULB) in March 2018. From September 2014 to August 2018, he was with the ICTEAM institute (UCL) and OPERA department (ULB) for part time. He is currently a Postdoctoral Researcher with the WiDeS Group, University of Southern California, Los Angeles, USA. He has been involved in many collaborations at the national, European, and international levels. From 2014 to 2015, he participated in the ICT-EMPhAtiC European project. During the years 2015–2018, he was a regular visitor of the Telecommunications Technological Center of Catalonia, Castelldefels, Spain, and the National Institute of Information and Communications Technology, Tokyo, Japan, in 2017. His current research interests lie in the design of mathematical models and algorithms to estimate, equalize, and synchronize communication signals.

Naokatsu Yamamoto received the B.S., M.S., and Ph.D. degrees in electrical engineering from Tokyo Denki University, Tokyo, Japan, in 1995, 1997, and 2000, respectively. From April 2000 to March 2001, he was a Research Associate with Tokyo Denki University. In April 2001, he joined the Communications Research Laboratory (now the National Institute of Information and Communications Technology), Tokyo, where he is currently the Director of Network Science and Convergence Device Technology Laboratory. He was also with Tokyo Denki University as a Visiting Associate Professor from May 2008 to June 2012 and the Ministry of Internal Affairs and Communications as a Deputy Director from July 2012 to September 2013. He proposed many types of novel crystal growth techniques and successfully developed a quantum dot (QD) optical frequency comb laser, an ultrabroadband QD light source, and a wavelength-tunable QD laser. He demonstrated successfully a high-speed and ultra-broadband photonic transport system constructed with novel nanostructured photonic devices. Recently, he has proposed the use of 1.0-μm waveband photonic transport systems to develop a novel optical frequency resource for optical communications. His research interests include nanostructured materials and III–V semiconductor QD and their photonic device applications in photonic transport systems.

Tetsuya Kawanishi (M'06–SM'06–F'13) received the B.E., M.E., and Ph.D. degrees in electronics from Kyoto University, Kyoto, Japan, in 1992, 1994, and 1997, respectively. From 1994 to 1995, he was with the Production Engineering Laboratory of Panasonic. During 1997, he was with the Venture Business Laboratory, Kyoto University, where he was involved in research on electromagnetic scattering and on near-field optics. In 1998, he joined the Communications Research Laboratory, Ministry of Posts and Telecommunications (now the National Institute of Information and Communications Technology), Tokyo, Japan. During 2004, he was a Visiting Scholar with the Department of Electrical and Computer Engineering, University of California at San Diego. Since April 2015, he has been a Professor with Waseda University, Tokyo. His current research interests include high-speed optical modulators and RF photonics.